Synthesis, Reactions, and Molecular and Electronic Structure of the Radical Cation $[Mo_2(\mu\text{-}C_8Me_8)(\eta\text{-}C_5H_5)_2]^+$: An Intermediate in the Redox Activation of an Alkyl C−H Bond

Neil G. Connelly,*,† Bernhard Metz,† A. Guy Orpen,† and Philip H. Rieger*,‡

School of Chemistry, University of Bristol, Bristol BS8 1TS, U.K., and Department of Chemistry, Brown University, Providence, Rhode Island 02912

Received July 11, 1995⊗

The reaction of $[Mo_2(\mu\text{-}C_8Me_8)(\eta\text{-}C_5H_5)_2]$ (**1**) with 1 equiv of $[Fe(\eta\text{-}C_5H_5)_2][PF_6]$ in CH_2Cl_2 gives $[Mo_2(\mu\text{-}C_8Me_8)(\eta\text{-}C_5H_5)_2][PF_6]$ ($\mathbf{1}^+[PF_6]^-$), which reacts with a second 1 equiv of $[Fe(\eta\text{-}C_5H_5)_2][PF_6]$ or 1 equiv of the trityl radical, $^\bullet CPh_3$, to give $[Mo_2(\mu\text{-}C_8Me_7CH_2)(\eta\text{-}C_5H_5)_2]^+$ ($\mathbf{2}^+$); depending on the oxidant the activation of one C−H bond of **1**, with the formation of $\mathbf{2}^+$, can occur by an EC or EEC mechanism. Complexes **1** and $\mathbf{1}^+$ constitute the first isolable redox pair to show the structural effects of one-electron oxidation on a metal−alkene bond. An X-ray crystal structure analysis shows that the geometry of $\mathbf{1}^+$ is similar to that of **1** and has approximate C_s symmetry. The Mo−Mo distance in $\mathbf{1}^+$ is consistent with the presence of a Mo═Mo double bond. The C_8 chain acts as a double μ-allylidene ligand while binding to Mo(2) as an η-alkene through C(4) and C(5). The Mo−C distances for atoms C(1), C(2), C(3), C(6), C(7), and C(8) of the C_8 chain are remarkably similar in **1** and $\mathbf{1}^+$ while the Mo(2)−C(4) and Mo(2)−C(5) distances are significantly increased and the C(4)−C(5) distance is decreased in $\mathbf{1}^+$ compared with that of **1**. These observed structural changes are consistent with a model for the bonding in the paramagnetic cation in which the unpaired electron occupies an orbital of a″ symmetry which is largely localized on Mo(2) and involved in π-back-bonding with the alkene function of the C_8Me_8 ligand in the classic Dewar−Chatt−Duncanson manner. This conclusion is supported by detailed NMR and ESR spectroscopic studies on **1** and $\mathbf{1}^+$ and by EHMO calculations.

Introduction

Electron-transfer reactions can provide a novel means by which the C−H bonds of hydrocarbons coordinated to mono- or polynuclear metal centers are activated. Studies of simple monometallic alkyls have been particularly useful in showing the effects of both the redox potential of the substrate and the nature of the oxidant on the mechanism of such C−H activation. Thus, the reaction of $[WMe_2(\eta\text{-}C_5H_5)_2]$ ($E^{o\prime} = -0.42$ V) with $[CPh_3]^+$ ($E^{o\prime} = ca.$ 0.3 V), to give $[WH(\eta\text{-}C_2H_4)(\eta\text{-}C_5H_5)_2]^+$, proceeds[1] by initial one-electron oxidation followed by H-atom abstraction, migratory insertion, and β-elimination. In this case, electron transfer is thermodynamically favored; $\Delta E^{o\prime}$ is *ca.* 0.7 V. One-electron oxidation also occurs as the first step in the reaction between $[ReR(PPh_3)(NO)(\eta\text{-}C_5H_5)]$ (R = alkyl) and $[CPh_3]^+$, to give[2] species such as $[Re(═CCR'R'')(PPh_3)(NO)(\eta\text{-}C_5H_5)]^+$; despite the unfavorability of electron transfer ($\Delta E^{o\prime}$ is *ca.* −0.2 V) the overall reaction is driven to completion by the H-atom abstraction. However, when the difference between the redox potentials is very unfavorable, as in $[FeR(CO)_2(\eta\text{-}C_5H_5)]$ and $[CPh_3]^+$ ($\Delta E^{o\prime}$ is *ca.* −1.0 V), products such as $[Fe(\eta\text{-}C_2H_4)(CO)_2(\eta\text{-}C_5H_5)]^+$ are formed[3] by direct hydride ion abstraction.

The redox activation of bi- and polynuclear metal−hydrocarbon complexes is potentially more complex in that multiple electron-transfer processes can be observed. For example, two mechanisms may be proposed for the oxidation of $[Ru_2(\mu\text{-}CH_2)(\mu\text{-}CO)(\mu\text{-}dppm)(\eta\text{-}C_5H_5)_2]$, $[Ru_3(\mu_3\text{-}CMe)(CO)_3(\eta\text{-}C_5Me_5)_3]$, and $[Mo_2(\mu\text{-}C_8Me_8)(\eta\text{-}C_5H_5)_2]$ (**1**, Scheme 1) to $[Ru_2(\mu\text{-}CH)(\mu\text{-}CO)(\mu\text{-}dppm)(\eta\text{-}C_5H_5)_2]^+$,[4] $[Ru_3(\mu_3\text{-}CCH_2)(CO)_3(\eta\text{-}C_5Me_5)_3]^+$,[5] and $[Mo_2(\mu\text{-}C_8Me_7CH_2)(\eta\text{-}C_5H_5)_2]^+$ [6] ($\mathbf{2}^+$, Scheme 1), respectively. For each of the three neutral molecules the cyclic voltammogram shows two oxidation waves. Accordingly, either an EC (E = electrochemical, C = chemical) pathway, where one-electron oxidation is followed by H-atom abstraction (as found for the mononuclear species described above), or an EEC mechanism, where the loss of two electrons is followed by proton elimination, is possible for C−H activation. In none of these cases, however, has a definitive distinction been made between the various possibilities. We give details,[7] therefore, of the synthesis and full characterization of the radical cation $\mathbf{1}^+$ (as its stable $[PF_6]^-$ salt) and

† University of Bristol. E-mail: N.G.C., Neil.connelly@bris.ac.uk; A.G.O., Guy.orpen@bris.ac.uk.
‡ Brown University. E-mail: Philip_Rieger@brown.edu.
⊗ Abstract published in *Advance ACS Abstracts,* December 15, 1995.

(1) Hayes, J. C.; Cooper, N. J. *J. Am. Chem. Soc.* **1982**, *104*, 5570.
(2) Bodner, G. S.; Gladysz, J. A.; Nielsen, M. F.; Parker, V. D. *J. Am. Chem. Soc.* **1987**, *109*, 1757.
(3) Bly, R. S.; Bly, R. K.; Hossain, M. M.; Silverman, G. S.; Wallace, E. *Tetrahedron* **1986**, *42*, 1093.
(4) Connelly, N. G.; Forrow, N. J.; Gracey, B. P.; Knox, S. A. R.; Orpen, A. G. *J. Chem. Soc., Chem. Commun.* **1985**, 14.
(5) Connelly, N. G.; Forrow, N. J.; Knox, S. A. R.; Macpherson, K. A.; Orpen, A. G. *J. Chem. Soc., Chem. Commun.* **1985**, 16.
(6) Bott, S. G.; Brammer, L.; Connelly, N. G.; Green, M.; Orpen, A. G.; Paxton, J. F.; Schaverien, C. J.; Bristow, S.; Norman, N. C. *J. Chem. Soc., Dalton Trans.* **1990**, 1957.
(7) Connelly, N. G.; Metz, B.; Orpen, A. G. *J. Chem. Soc., Chem. Commun.* **1994**, 2109.

0276-7333/96/2315-0729$12.00/0

Scheme 1

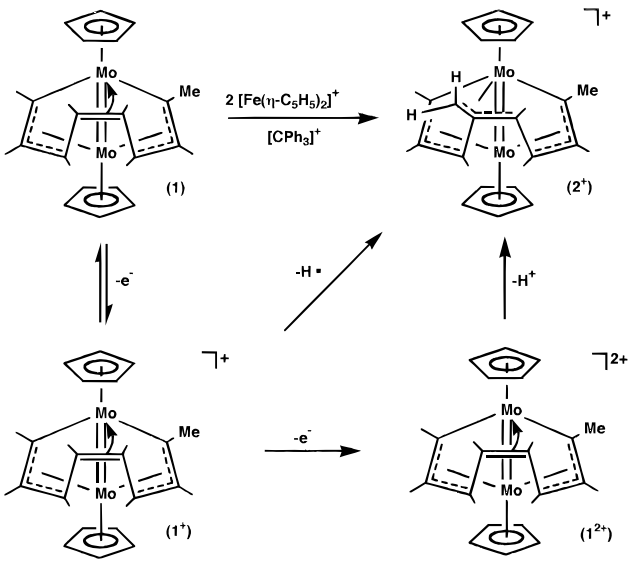

studies of its reactions with the $^{\bullet}CPh_3$ radical and with $[Fe(\eta\text{-}C_5H_5)_2]^+$ which show that the mechanism of the C−H activation of **1** is dependent not only on the redox potentials of the reactants but also on the nature of the chemical oxidant. Furthermore, an X-ray structural study of $\mathbf{1}^+$, in conjunction with ESR and NMR spectroscopy and extended Hückel molecular orbital (EHMO) calculations, has provided insight into the electronic structures of the redox pair $\mathbf{1}/\mathbf{1}^+$.

Results and Discussion

Synthesis and Reactions of $[Mo_2(\mu\text{-}C_8Me_8)(\eta\text{-}C_5H_5)_2][PF_6]$ ($\mathbf{1}^+$). The cyclic voltammogram of **1**[6] shows two oxidation waves in the range −1.5 to 1.5 V. The first is fully reversible ($E^{\circ\prime} = -0.13$ V) whereas the second is completely irreversible [$(E_p)_{ox} = 0.70$ V; scan rate = 200 mV s^{-1}] for scan rates up to 1 V s^{-1}. On treatment of **1** with 2 equiv of $[Fe(\eta\text{-}C_5H_5)_2][PF_6]$, high yields of purple $\mathbf{2}^+$ have been isolated.[6] However, on addition of 1 equiv of the oxidant to **1** in CH_2Cl_2, a brown solution is rapidly formed from which dark brown crystals of $\mathbf{1}^+$, as the $[PF_6]^-$ salt, are readily isolated. The salt $[Mo_2(\mu\text{-}C_8Me_8)(\eta\text{-}C_5H_5)_2][PF_6]$ was characterized by elemental analysis (C and H) and by cyclic voltammetry, which showed one reversible reduction wave and one irreversible oxidation wave at potentials essentially identical to those of the two oxidation waves of **1**. The further characterization of $\mathbf{1}^+$, by X-ray crystallography and ESR and NMR spectroscopy, is discussed below.

The isolation of $\mathbf{1}^+$ provided the ideal means by which the mechanism of the oxidative activation of **1** could be probed. Thus, the reaction of $\mathbf{1}^+$ in CH_2Cl_2 with 1 equiv of either $[Fe(\eta\text{-}C_5H_5)_2][PF_6]$ or $^{\bullet}CPh_3$ [generated by dissolving 4-(triphenylmethyl)-1-(diphenylmethylidene)-2,5-cyclohexadiene] gave a purple solution from which a high yield of $\mathbf{2}^+$, as the $[PF_6]^-$ salt, was isolated and identified by NMR spectroscopy.[6] These reactions show conclusively that, in the case of **1** and by implication in the cases of $[Ru_2(\mu\text{-}CH_2)(\mu\text{-}CO)(\mu\text{-dppm})(\eta\text{-}C_5H_5)_2]$[4] and $[Ru_3(\mu_3\text{-}CCH_3)(CO)_3(\eta\text{-}C_5Me_5)_3]$,[5] both EC and EEC mechanisms are possible, depending at least in part on the oxidant. The EEC mechanism clearly operates in the reaction of $[Fe(\eta\text{-}C_5H_5)_2][PF_6]$ with **1**. As **1** gives a quantitative yield of $\mathbf{2}^+$ when treated with *1* equiv of $[CPh_3]^+$, however, an EC mechanism is more likely (though the additional participation of the EEC process cannot be discounted when an excess of the oxidant is used).

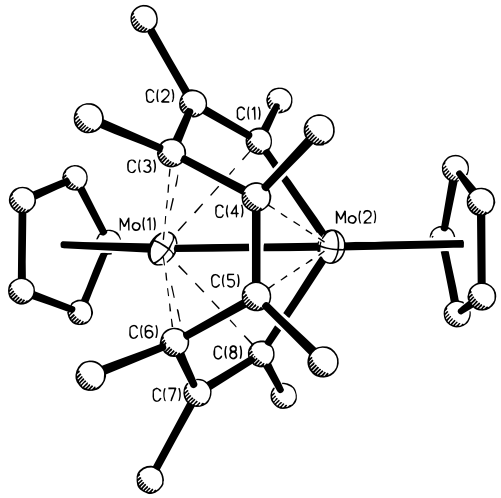

Figure 1. Molecular structure of $[Mo_2(\mu\text{-}C_8Me_8)(\eta\text{-}C_5H_5)_2]^+$ ($\mathbf{1}^+$).

Table 1. Selected Bond Lengths (Å) and Angles (deg) for $[Mo_2(\mu\text{-}C_8Me_8)(\eta\text{-}C_5H_5)_2][PF_6]$ ($\mathbf{1}^+[PF_6]^-$)

Mo(1)−C(1)	2.252(5)	Mo(1)−C(2)	2.343(5)	Mo(1)−C(3)	2.303(4)
Mo(1)−C(6)	2.292(5)	Mo(1)−C(7)	2.342(5)	Mo(1)−C(8)	2.252(5)
Mo(1)−Mo(2)	2.6199(8)	Mo(2)−C(1)	2.094(5)	Mo(2)−C(4)	2.402(4)
Mo(2)−C(5)	2.407(4)	Mo(2)−C(8)	2.098(5)	C(1)−C(1′)	1.520(7)
C(1)−C(2)	1.427(7)	C(2)−C(2′)	1.515(7)	C(2)−C(3)	1.426(7)
C(3)−C(3′)	1.528(6)	C(3)−C(4)	1.530(6)	C(4)−C(4′)	1.518(6)
C(4)−C(5)	1.394(6)	C(5)−C(5′)	1.524(6)	C(5)−C(6)	1.510(6)
C(6)−C(6′)	1.531(6)	C(6)−C(7)	1.441(6)	C(7)−C(7′)	1.528(6)
C(7)−C(8)	1.412(7)	C(8)−C(8′)	1.526(6)		

C(8)−Mo(1)−Mo(2)	50.32(12)	C(1)−Mo(1)−Mo(2)	50.22(13)
C(6)−Mo(1)−Mo(2)	74.99(11)	C(3)−Mo(1)−Mo(2)	75.32(12)
C(7)−Mo(1)−Mo(2)	73.86(12)	C(2)−Mo(1)−Mo(2)	74.16(13)
C(1)−Mo(2)−Mo(1)	55.73(13)	C(8)−Mo(2)−Mo(1)	55.70(13)
C(4)−Mo(2)−Mo(1)	72.34(11)	C(5)−Mo(2)−Mo(1)	72.03(11)
C(2)−C(1)−C(1′)	120.4(5)	C(2)−C(1)−Mo(2)	115.6(3)
C(1′)−C(1)−Mo(2)	123.6(4)	C(2)−C(1)−Mo(1)	75.4(3)
C(1′)−C(1)−Mo(1)	126.1(4)	Mo(2)−C(1)−Mo(1)	74.0(2)
C(3)−C(2)−C(1)	115.5(4)	C(3)−C(2)−C(2′)	121.3(4)
C(1)−C(2)−C(2′)	123.2(5)	C(3)−C(2)−Mo(1)	70.6(3)
C(1)−C(2)−Mo(1)	68.5(3)	C(2′)−C(2)−Mo(1)	130.1(4)
C(2)−C(3)−C(3′)	119.8(4)	C(2)−C(3)−C(4)	116.3(4)
C(3′)−C(3)−C(4)	113.7(4)	C(2)−C(3)−Mo(1)	73.7(3)
C(3′)−C(3)−Mo(1)	127.4(3)	C(4)−C(3)−Mo(1)	99.6(3)
C(5)−C(4)−C(4′)	125.2(4)	C(5)−C(4)−C(3)	115.5(4)
C(4′)−C(4)−C(3)	116.8(4)	C(5)−C(4)−Mo(2)	73.3(2)
C(4′)−C(4)−Mo(2)	114.1(3)	C(3)−C(4)−Mo(2)	97.8(3)
C(4)−C(5)−C(6)	116.7(4)	C(4)−C(5)−C(5′)	124.0(4)
C(6)−C(5)−C(5′)	117.5(4)	C(4)−C(5)−Mo(2)	73.0(2)
C(6)−C(5)−Mo(2)	97.4(3)	C(5′)−C(5)−Mo(2)	112.5(3)
C(7)−C(6)−C(5)	117.0(4)	C(7)−C(6)−C(6′)	120.4(4)
C(5)−C(6)−C(6′)	113.2(4)	C(7)−C(6)−Mo(1)	73.8(3)
C(5)−C(6)−Mo(1)	100.3(3)	C(6′)−C(6)−Mo(1)	125.7(3)
C(8)−C(7)−C(6)	115.3(4)	C(8)−C(7)−C(7′)	123.4(4)
C(6)−C(7)−C(7′)	121.3(4)	C(8)−C(7)−Mo(1)	68.6(3)
C(6)−C(7)−Mo(1)	70.0(3)	C(7′)−C(7)−Mo(1)	130.3(4)
C(7)−C(8)−C(8′)	120.3(4)	C(7)−C(8)−Mo(2)	115.5(3)
C(8′)−C(8)−Mo(2)	123.6(4)	C(7)−C(8)−Mo(1)	75.6(3)
C(8′)−C(8)−Mo(1)	127.2(4)	Mo(2)−C(8)−Mo(1)	74.0(2)

X-ray Structure of $[Mo_2(\mu\text{-}C_8Me_8)(\eta\text{-}C_5H_5)_2][PF_6]$: Bonding in Metal−Alkene Complexes. Crystals of $[Mo_2(\mu\text{-}C_8Me_8)(\eta\text{-}C_5H_5)_2][PF_6]$ suitable for an X-ray diffraction study were grown by allowing diethyl ether to diffuse into a solution of $\mathbf{1}^+$ in CH_2Cl_2. The structural analysis shows that the geometry of $\mathbf{1}^+$ (Figure 1, Table 1) is similar to that of **1**[8] and has approximate C_s symmetry. In both **1** and $\mathbf{1}^+$ the C_8 chain is η^3-coordinated to Mo(1) through C(1-3) and C(6-8) and

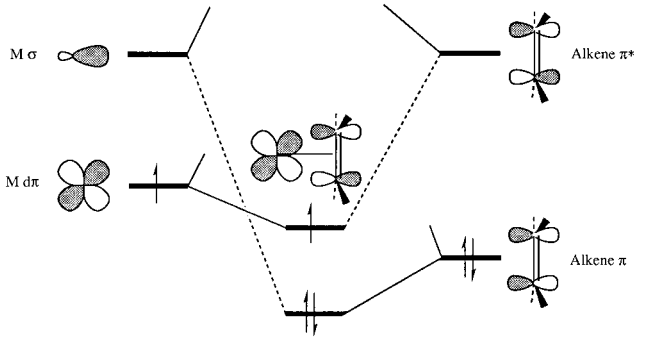

Figure 2. Schematic orbital interaction diagram for the three-electron Dewar−Chatt−Duncanson metal−alkene bond in $\mathbf{1}^+$.

σ-bonded to Mo(2) through C(1) and C(8), thereby acting as a double μ-allylidene ligand while binding to Mo(2) as an η-alkene through C(4) and C(5). As in **1** the Mo−Mo distance in $\mathbf{1}^+$ is consistent with the presence of a Mo═Mo double bond [Mo(1)−Mo(2) 2.620(1) Å; *cf.* 2.595(1) Å in **1** and 2.655(1) Å in $\mathbf{2}^+$]. Furthermore, the Mo−C distances for atoms C(1), C(2), C(3), C(6), C(7), and C(8) of the C_8 chain are remarkably similar in **1** and $\mathbf{1}^+$ [bond lengths in $\mathbf{1}^+$ averaged over C_s symmetry are Mo(1)−C(1) 2.252(5), Mo(1)−C(2) 2.343(5), Mo(1)−C(3) 2.298(5), and Mo(2)−C(1) 2.096(5) Å; *cf.* 2.237(2), 2.348(2), 2.317(2), and 2.093(2) Å, respectively, in **1**]. By contrast, the Mo(2)−C(4) and Mo(2)−C(5) distances are significantly increased in $\mathbf{1}^+$ [mean 2.405(5) Å] as compared with **1** [2.234(2) Å]. In **1** this interaction is essentially an isolated metal−alkene bond of the classic Dewar−Chatt−Duncanson type. In $\mathbf{1}^+$ the metal−alkene bond is clearly weakened and the C(4)−C(5) bond slightly strengthened [1.394(6) Å; *cf.* 1.442(3) Å in **1**] as a result of oxidation. These changes are consistent with the depopulation, on oxidation, of the orbital (the HOMO) involved in Mo(2)−alkene-π* back-donation, which, as shown in Figure 2, has a″ symmetry. Thus the metal−alkene bond in $\mathbf{1}^+$ may be described as a three-electron interaction (Figure 2), observable in this case because of the constraints imposed by the C_8 chain conformation.

EHMO Calculations. EHMO calculations were carried out on $[Mo_2(\mu\text{-}C_8H_8)(\eta\text{-}C_5H_5)_2]^+$, a model for cation $\mathbf{1}^+$, with geometry based on that observed in the crystal structure but with exact C_s symmetry imposed and using parameters taken from the literature.[9] The axis system used (Figure 3) has the molecular *x* axis parallel to the Mo−Mo vector and the *z* axis parallel to the C(4)−C(5) bond. The energy levels of the frontier occupied orbitals are closely spaced, there being two other orbitals calculated to lie within 0.45 eV of the HOMO which lies 0.94 eV below the LUMO. All these orbitals are predominantly Mo 4d in character. The calculated HOMO has a′ symmetry and is Mo−Mo σ-bonding in character. It is composed primarily of equal contributions from each molybdenum atom (mainly $d_{x^2-y^2}$ and d_{xy}; see Figure 3a). The next highest energy orbital (*ca.* 0.06 eV below the HOMO) is of a″ symmetry and is largely localized on Mo(2) (primarily d_{yz} with very small p_z and d_{xz} contributions) with a significant contribution from the alkene π* orbital [*i.e.* primarily C(4) and C(5) p_y with some p_x] so as to give this orbital

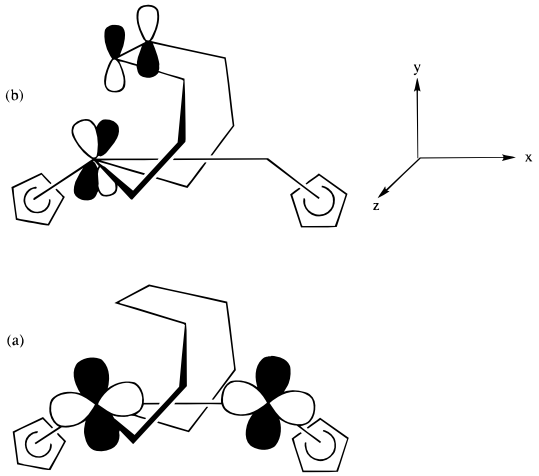

Figure 3. Schematic illustration of the calculated highest (a) and second highest (b) occupied molecular orbitals for $[Mo_2(\mu\text{-}C_8H_8)(\eta\text{-}C_5H_5)_2]^+$ by EHMO methods, showing the principal orbital contributions (not to scale) and the axis system used.

Mo(2)−alkene bonding character (see Figure 3b). This clearly corresponds to the molecular orbital characteristics predicted on the basis of the structure analysis above and analysis of the ESR spectrum (see below). Apparently the EHMO calculations do not correctly predict the ordering of the two highest occupied orbitals, presumably because of the inadequacy of the parameters used in the calculations.[10]

Distribution of Unpaired Electron Density in $\mathbf{1}^+$. The results of the X-ray structure determination and of the EHMO studies described above point strongly to the SOMO of $\mathbf{1}^+$ having the characteristics illustrated in Figure 3b. ESR and NMR spectroscopic studies on $\mathbf{1}^+$ have shed further light on the distribution of the unpaired electron density in the paramagnetic cation.

ESR Spectroscopy. Analysis of ESR Spectra. The ESR spectrum of $\mathbf{1}^+$ in CH_2Cl_2/thf at 180 K (Figure 4a) consists of a central 1:6:15:20:15:6:1 multiplet arising from hyperfine coupling to six equivalent protons (two methyl groups). Surrounding the central multiplet are four weak satellites resulting from hyperfine coupling to Mo (^{95}Mo, 15.9%, and ^{97}Mo, 9.6%; $I = {}^5/_2$, $\mu_{97}/\mu_{95} = 1.014$). Because of differences in line width, amplitude ratios are not a reliable measure of relative intensities, and overlap precludes an accurate integration of single features. Thus it was not immediately clear whether coupling is to a single Mo nucleus or to two approximately equivalent Mo nuclei. Accordingly, the wings of the spectrum were examined carefully under high amplification; if both Mo nuclei were coupled, a further set of weaker satellites would have been observable with good signal-to-noise ratio. No other satellites were detected, and we conclude that the observed coupling is to only one Mo nucleus. Analysis of the spectrum gives $\langle g \rangle$, $\langle A^{Mo} \rangle$, and $\langle A^H \rangle$ (Table 2).

The spectrum of $\mathbf{1}^+$ in CH_2Cl_2/thf (1:2) at 77 K (Figure 4b) is qualitatively similar to the isotropic spectrum but with more widely spaced ^{95,97}Mo satellites. The central feature contains all three *g*-components; each component shows proton hyperfine coupling, but only for the central component is the structure well resolved as a

(8) Green, M.; Norman, N. C.; Orpen, A. G.; Schaverien, C. J. *J. Chem. Soc., Dalton Trans.* **1984**, 2455.

(9) Alvarez, S. *Tables of Parameters for Extended Hückel Calculations*; University of Barcelona: Barcelona, 1989.

(10) Calculations using the CAChe parameter set (CAChe Scientific, Inc.) gave the same ordering of the orbitals but with the a″ MO 0.30 eV below the a′ HOMO.

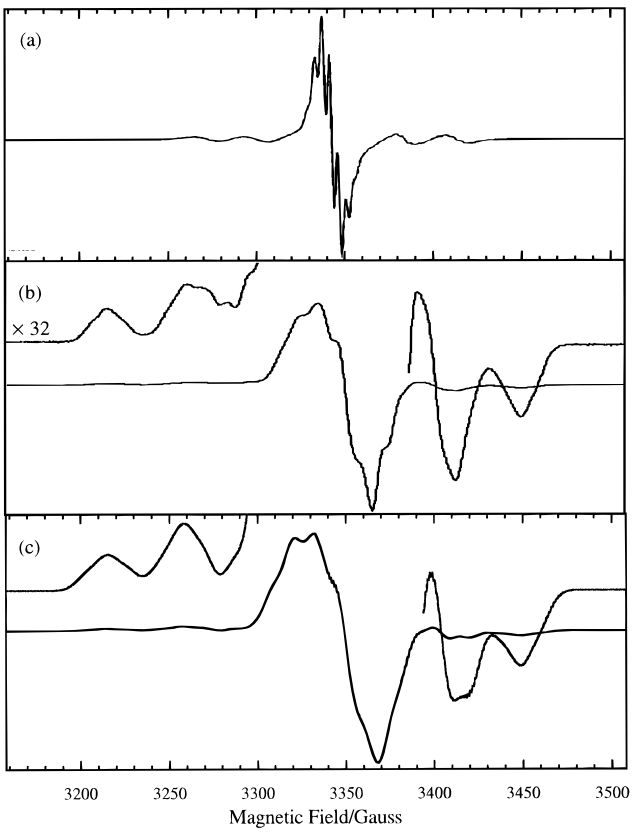

Figure 4. ESR spectrum of $\mathbf{1}^+$ in CH_2Cl_2/thf: (a) Isotropic spectrum at 180 K; (b) frozen solution spectrum at 77 K (the ^{95,97}Mo satellites were recorded with the gain increased by a factor of 32); (c) computer simulation of frozen-solution spectrum using the parameters shown in Table 2, with isotropic coupling to two ^{1}H nuclei and Gaussian line widths of 5.0 G (central feature) and 6.0 G (satellites).

Table 2. ESR Parameters for $[Mo_2(\mu\text{-}C_8Me_8)(\eta\text{-}C_5H_5)_2]^+$ ($\mathbf{1}^+$)[a]

	g	A^{Mo}	A^H
isotropic	2.0139(1)	26.66(3)	3.99(5)
x[b]	2.030(1)	42.2(1)	
y[b]	2.0118(2)	25.1(1)	10.6(1)
z	2.000(2)	12.7(2)	

[a] Hyperfine couplings in units of 10^{-4} cm^{-1}. [b] g and A^{Mo} principal axes differ by 38 ± 2°.

1:2:1 triplet [g_y = 2.0118, A_y^H = (10.6 ± 0.1) × 10^{-4} cm^{-1}]. The same structure is resolved on one of the low-field satellites (assigned to g_y) and poorly developed shoulders on another satellite (assigned to g_x) suggest a comparable coupling. It is likely that the proton hyperfine interaction is nearly isotropic. The observed coupling to only two protons at 77 K, together with the increase in coupling by almost a factor of 3, suggests that methyl group rotation is frozen out at low temperatures such that four of the six protons have negligible couplings.

The shapes and positions of the ^{95,97}Mo satellites in the frozen solution spectrum are easily understood, at least qualitatively. The outer pair of satellites corresponds to $m_I = \pm 5/2$ and the largest Mo hyperfine component (A_x). The inner pair is a superposition of $m_I = \pm 3/2$ (A_x) and $\pm 5/2$ (A_y); the high-field member of this pair also has a contribution from $m_I = -5/2$ (A_z). The centers of the A_x and A_y pairs correspond to g = 2.023 and 2.019, respectively, both larger than g_y measured for the central feature. This discrepancy can be understood if it is assumed that the x and y principal axes of the g- and A-matrices are displaced by the angle α. If g_y is fixed, the satellites can be fitted to give the values of g_x, A_x, A_y, and α listed in Table 2; values of g_z and A_z, also given in Table 2, were computed from $\langle g\rangle$ and $\langle A^{Mo}\rangle$. A computer-simulated spectrum based on these parameters is shown in Figure 4c.

Interpretation of ESR Parameters. If we assume that the SOMO is of a″ symmetry with a $4d_{yz}$ metal contribution, eq 1,as illustrated in Figures 2 and 3b and

$$|\mathrm{SOMO}\rangle = a|yz\rangle + \ldots \quad (1)$$

as suggested by the X-ray study, the components of the hyperfine coupling matrix are given by eqs 2,[11]where P

$$A_x = A_s - {}^4/_7 Pa^2 \quad (2a)$$

$$A_y = A_z = A_s + {}^2/_7 Pa^2 \quad (2b)$$

$$A_s = \langle A\rangle - P\Delta\langle g\rangle = 27.25 \times 10^{-4}\ \mathrm{cm}^{-1} \quad (2c)$$

(=−50.7 × 10^{-4} cm^{-1}) is the average dipolar coupling parameter for ^{95}Mo and ^{97}Mo[12] and A_s is the contact term, given by eq 2c.[13] Equation 2b predicts an axial hyperfine matrix, quite different from the experimental result. In an attempt to explain this discrepancy, we have applied spin−orbit coupling corrections to obtain the g-matrix components given by (3), where ζ is the

$$g_{xx} = g_e + 2\zeta\sum_{i\neq 0}\frac{a^2(c^i_{x^2-y^2} + \sqrt{3}c^i_{z^2})^2}{E_0 - E_i} \quad (3a)$$

$$g_{yy} = g_e + 2\zeta\sum_{i\neq 0}\frac{a^2(c^i_{xy})^2}{E_0 - E_i} \quad (3b)$$

$$g_{zz} = g_e + 2\zeta\sum_{i\neq 0}\frac{a^2(c^i_{xz})^2}{E_0 - E_i} \quad (3c)$$

$$g_{xy} = 2\zeta\sum_{i\neq 0}\frac{a^2 c^i_{xy}(c^i_{x^2-y^2} + \sqrt{3}c^i_{z^2})}{E_0 - E_i} \quad (3d)$$

spin−orbit coupling parameter for Mo, E_i is the energy of the MO, and, for example, c^i_{xy} is the LCAO coefficient of d_{xy} in the ith MO. The g-matrix is diagonalized by rotation about the z-axis by the angle α_g, given by eq 4.

$$\tan 2\alpha_g = \frac{2g_{xy}}{g_{xx} - g_{yy}} \quad (4)$$

If we assume that the major contributions to g_{xx}, g_{yy}, and g_{xy} are due to spin−orbit coupling with a single doubly-occupied a′ MO just below the SOMO, eq 4 reduces to eq 5a, where R is given by eq 5b. If we further assume that $\alpha_g = \alpha_{exptl}$, eq 5a gives R = 1.3, in reasonable agreement with EHMO calculations for the

$$\tan 2\alpha_g \approx \frac{2R}{R^2 - 1} \quad (5a)$$

$$R = \frac{c^i_{x^2-y^2} + \sqrt{3}c^i_{z^2}}{c^i_{xy}} \quad (5b)$$

(11) Peake, B. M.; Rieger, P. H.; Robinson, B. H.; Simpson, J. J. *Am. Chem. Soc.* **1980**, *102*, 156.
(12) Morton, J. R.; Preston, K. F. *J. Magn. Reson.* **1978**, *30*, 577.

Scheme 2. Numbering Scheme for NMR Spectra of 1 and 1^+

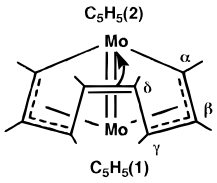

predicted HOMO, $R = 0.85$. Since $g_z - g_e$ is very small, it appears that spin−orbit coupling to a″ orbitals with d_{xz} character is negligible, and EHMO calculations support this conclusion. Again assuming that $\alpha_g = 38°$, we obtain $g_{xx} = 2.023$, $g_{yy} = 2.019$, and $g_{xy} = 0.0088$.

Ignoring spin−orbit coupling to a″ MO's, we obtain the spin−orbit coupling corrections to the Mo hyperfine coupling components shown in eqs 6, where $\Delta g_i = g_i - g_e$. Note that the correction terms represented by sums in eqs 6b,c cannot be related to *g*-matrix components and thus are independent parameters.

$$(A_{xx})_{corr} = P[\Delta g_{xx} + {}^3/_{14}\Delta g_{yy}] \qquad (6a)$$

$$(A_{yy})_{corr} - (A_{zz})_{corr} = P\left[{}^3/_7\Delta g_{xx} + {}^{17}/_{14}\Delta g_{yy} - \frac{2\sqrt{3}}{7}a^2\zeta\sum_{i\neq 0}\frac{c^i_{z^2}(c^i_{x^2-y^2} + \sqrt{3}c^i_{z^2})}{E_0 - E_i}\right] \qquad (6b)$$

$$(A_{xy})_{corr} = P\left({}^{11}/_{14}g_{xy} + {}^2/_7\zeta\sum_{i\neq 0}\frac{\sqrt{3}a^2c^i_{xy}c^i_{z^2}}{E_0 - E_i}\right) \qquad (6c)$$

The principal axes of the hyperfine tensor are rotated from the molecular *x*- and *y*-axes by the angle α_A, given by eq 7. However, since $A_{xx} - A_{yy}$ is probably large

$$\tan 2\alpha_A = \frac{2A_{xy}}{A_{xx} - A_{yy}} \qquad (7)$$

compared with A_{xy}, it is reasonable to assume that the hyperfine principal axes are essentially molecular axes. Equations 2a and 6a, together with A_{xx}, A_s, and the above values of Δg_{xx} and Δg_{yy}, then give $a^2 = 0.56$, in good agreement with the EHMO result, $a^2 = 0.59$. The lead terms of eq 6b give a contribution of -1.5×10^{-4} cm^{-1}, of opposite sign and considerably smaller than the experimental value of $A_{yy} - A_{zz}$. The remaining correction term is not easily estimated, but it is probably also negative. This discrepancy suggests that either there is another contribution to $A_{yy} - A_{zz}$, perhaps $5p_z$ character in the SOMO, or that the value of A_{zz} computed from A_{xx}, A_{yy}, and $\langle A\rangle$ has a significant error, possibly resulting from the temperature-dependence of $\langle A\rangle$.[14]

We turn now to the proton coupling in the ESR spectrum of $\mathbf{1}^+$. On the basis of the crystallographic study, the δ methyl protons (labeling as in Scheme 2) would appear the most likely to couple with the unpaired electron. However, labeling the δ carbon atom substituents has shown this not to be the case: oxidation of $[Mo_2(\mu\text{-}C_8Me_7CH_2D)(\eta\text{-}C_5H_5)_2]$ and $[Mo_2(\mu\text{-}C_8Me_7\text{-}Et)(\eta\text{-}C_5H_5)_2]$, with D and Me substituted at one of the δ-methyl positions, respectively,[6] gave $[Mo_2(\mu\text{-}C_8Me_7\text{-}CH_2D)(\eta\text{-}C_5H_5)_2]^+$ and $[Mo_2(\mu\text{-}C_8Me_7Et)(\eta\text{-}C_5H_5)_2]^+$, the ESR spectra of which were identical to that of $\mathbf{1}^+$. Thus, in order to assign the proton coupling, the ^{1}H NMR spectra of **1** and $\mathbf{1}^+$ have been studied, both individually and as mixtures in solution.

Table 3. ^{1}H NMR Spectroscopic Data (ppm) for $[Mo_2(\mu\text{-}C_8Me_8)(\eta\text{-}C_5H_5)_2]$ (1) and $[Mo_2(\mu\text{-}C_8Me_8)(\eta\text{-}C_5H_5)_2]^+$ (1^+) in CD_2Cl_2 at 293 K

signal	**1**	$\mathbf{1}^+$ [a]	δ_{para}
Me_α	2.42		
Me_β	2.39	13.44 (*ca.* 1.3)[b]	11.05
Me_γ	1.97	*ca.* 32	*ca.* 30.0
Me_δ	0.80	13.4[c]	12.6
	0.76[d]	13.37 (40 Hz)[d]	12.61[d]
Cp(1)	4.03	−8.34 (1.8)	−12.37
Cp(2)	5.06	10.15 (0.4)	5.09

[a] Peak width at half-height, in kHz unless otherwise stated, given in parentheses. [b] The signal tentatively assigned to Me_β could be due to Me_α (see text). [c] Estimated from the corresponding ^{2}H signal of $[Mo_2(\mu\text{-}C_8Me_7CH_2D)(\eta\text{-}C_5H_5)_2]^+$; the ^{1}H signal could not be detected directly. [d] ^{2}H signal for the CH_2D analogue.

NMR Spectroscopy. In order to study the ^{1}H NMR spectrum of the paramagnetic cation $\mathbf{1}^+$, a definitive assignment of the four methyl and two Cp resonances observed[8] in the ^{1}H NMR spectrum of **1** was first required. The signal due to Me_δ was previously assigned on the basis of deuteration studies.[6] The remaining three methyl signals have now been assigned by means of ^{1}H NOE experiments (Table 3). Thus, irradiation in turn at H_δ, H_γ, H_β, and H_α led to enhancement of the signals due to H_γ, H_β (and H_δ), H_α (and H_γ), and H_β, respectively. In addition, the proton signals of Cp(2) and Cp(1) were enhanced on irradiation at H_δ and H_γ, respectively.

As expected for a paramagnetic complex, the absorptions in the ^{1}H NMR spectrum of $\mathbf{1}^+$ are much broader than those of **1** and at room temperature in CD_2Cl_2 only three signals are observed in the range −400 to 400 ppm (Table 3). In order to assign these signals, and in an attempt to detect the three other expected resonances [there are four inequivalent methyl groups and two inequivalent C_5H_5 rings in $\mathbf{1}^+$], the ^{1}H NMR spectra of mixtures containing varying relative concentrations of **1** and $\mathbf{1}^+$ were obtained; because **1** and $\mathbf{1}^+$ undergo fast, reversible electron exchange, the ^{1}H NMR spectra of the mixtures show an averaged set of signals rather than a superimposition of the two individual spectra. Plots of the chemical shifts of the individual signals *vs* the mole fraction of the cation $\mathbf{1}^+$ are close to linear. Thus, the signals observed at −8.34 and 10.15 ppm in the spectrum of $\mathbf{1}^+$ are linked to those of Cp(1) and Cp(2), respectively, for the neutral complex **1**. The third (and broadest) signal, at 13.44 ppm, is due to either Me_α or Me_β, but the close proximity of the corresponding signals for **1** does not allow unambiguous assignment by extrapolation. No signal for Me_γ of $\mathbf{1}^+$ is observed for mole fractions of the cation above 0.04, and at such low values the correlation between mole fraction and chemical shift deviates from linearity for all signals (because of the inherent imprecision in sample weighing). However, it was possible to achieve a linear correlation in

(13) The signs of A_x, A_y, A_z, and $\langle A\rangle$ are necessarily the same; to be consistent with eq 2a, we assume positive signs.

(14) Inclusion of d_{xz} character in the SOMO would lead to a negative contribution to A_{yy}, apparently resolving the discrepancy. However, d_{xz} character would also contribute to A_{yy} and the resulting matrix, when diagonalized, would again be axial; spin−orbit coupling corrections are considerably more complex but do not appear to clarify the matter.

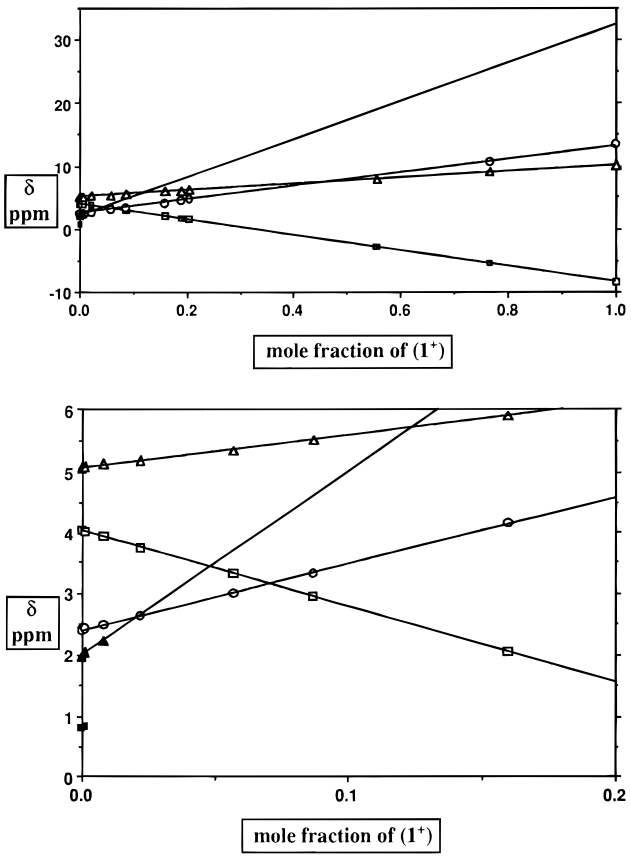

Figure 5. Plot of observed ^{1}H NMR chemical shift *vs* mole fraction of $\mathbf{1}^+$ for mixtures of **1** and $\mathbf{1}^+$ in CH_2Cl_2: (a, top) mole fraction 0.0−1.0; (b, bottom) mole fraction 0.0−0.2. Key: △ = C_5H_5(2), □ = C_5H_5(1), ● = α, ○ = β, ▲ = γ, ■ = δ.

this region by using the signal for Cp(1) as an internal standard for the relative concentrations of $\mathbf{1}^+$ and **1**. Thus, Figure 5 shows the plot of observed chemical shift *vs* mole fraction calculated from the observed chemical shift for Cp(1). Extrapolation to zero concentration of **1** from the data for mixtures of **1** and $\mathbf{1}^+$ then provides a value of *ca.* 32 (±2.5) ppm for the chemical shift of Me_γ in $\mathbf{1}^+$. The ^{1}H signal for the Me_δ protons of **1** is broadened even at very low relative concentrations of $\mathbf{1}^+$. However, a reliable estimate of the chemical shift can be made from the ^{2}H NMR spectrum of the cation. The ^{1}H chemical shift and the ^{2}H chemical shift for analogous protio and deutero complexes, such as $\mathbf{1}^+$ and $[Mo_2(\mu\text{-}C_8Me_7CH_2D)(\eta\text{-}C_5H_5)_2]^+$, are expected to be very similar.[15,16] For example, the Me_δ protons for **1** are observed at 0.80 ppm and the deuterium signal for the CH_2D_δ group in $[Mo_2(\mu\text{-}C_8Me_7CH_2D)(\eta\text{-}C_5H_5)_2]]$ is observed at 0.76 ppm. Moreover, the ^{2}H NMR signal for the paramagnetic cation is expected to be much sharper (*ca.* 42 times[15,17]). Thus, the ^{2}H NMR spectrum of $[Mo_2(\mu\text{-}C_8Me_7CH_2D)(\eta\text{-}C_5H_5)_2]^+$ (deuterium at Me_δ) shows a broad signal at 13.37 ppm (even though the methyl group is only partially deuterated); a similar chemical shift (±2 ppm) can be assigned to Me_δ for $\mathbf{1}^+$ [18] (coincidentally similar to that of the broad resonance assigned to Me_α/Me_β).

The chemical shift differences, δ_{para}, between the ^{1}H NMR signals for **1** and $\mathbf{1}^+$, the paramagnetic shifts, are given in Table 3. On the basis of eq 8,the isotropic ^{1}H

$$\delta_{para} = -a\frac{\gamma_e}{\gamma_p}\frac{g\mu_B S(S+1)}{3kT} \qquad (8)$$

hyperfine coupling (4.24 G) observed in the ESR spectrum of $\mathbf{1}^+$ corresponds to an isotropic paramagnetic shift of the order of ±320 ppm. None of the paramagnetic shifts in Table 3 is large enough to account for the ESR spectrum. We deduce, therefore, that the protons of either Me_α or Me_β (which cannot be distinguished but one of which gives the signal at 13.44 ppm) are responsible for the ^{1}H coupling in the ESR spectrum. Intuitively, the Me_α groups [those of the carbon atoms σ-bound to Mo(2)] are favored.

Conclusions

(i) A stable $[PF_6]^-$ salt of the radical cation $[Mo_2(\mu\text{-}C_8Me_8)(\eta\text{-}C_5H_5)_2]^+$ has been isolated; its reactions with $[Fe(\eta\text{-}C_5H_5)_2]^+$ and 4-(triphenylmethyl)-1-(diphenylmethylidene)-2,5-cyclohexadiene (as a source of the radical $^\bullet CPh_3$) show that the oxidative activation of one C−H bond of **1** can occur by either EC or EEC processes, depending on the oxidant.

(ii) Complexes **1** and $\mathbf{1}^+$ constitute the first structurally characterized redox pair containing a metal−alkene bond. X-ray diffraction studies on $[Mo_2(\mu\text{-}C_8Me_8)(\eta\text{-}C_5H_5)_2][PF_6]$ show a lengthening of the Mo−C_{alkene} bonds and a shortening of the coordinated C=C bond on oxidation of **1**, consistent with the Dewar−Chatt−Duncanson model for metal−alkene bonding.

(iii) NMR and ESR spectroscopic studies on **1** and $\mathbf{1}^+$, coupled with EHMO calculations, are also consistent with a model for the bonding in the paramagnetic cation in which the unpaired electron occupies an orbital of a″ symmetry, largely localized on Mo(2) and involved in π-back-bonding with the alkene function of the C_8Me_8 ligand with some delocalization.

Experimental Section

The preparation, purification, and reactions of the complexes described were carried out under an atmosphere of dry nitrogen using dried, distilled, and deoxygenated solvents. Unless stated otherwise, the complexes are air-stable in the solid state and dissolve in polar solvents such as CH_2Cl_2 and thf to give solutions which only slowly decompose in air. ^{1}H and ^{2}H NMR spectra and ^{1}H NOE experiments were recorded on a Jeol GX 400 spectrometer. X-band ESR spectra were recorded on a Bruker ESP-300E spectrometer equipped with a Bruker variable-temperature accessory and a Hewlett Packard 5350B microwave frequency counter. The field calibration was checked by measuring the resonance of the diphenylpicrylhyrazyl (dpph) radical before each series of spectra. Electrochemical studies were carried out as described previously.[19] All potentials were calibrated using ferrocene as an internal standard. Under the conditions used, $E°'$ for the couple $[Fe(\eta\text{-}C_5H_5)_2]^+/[Fe(\eta\text{-}C_5H_5)_2]$ was 0.47 V. Microanalyses were carried out by the staff of the Microanalytical Service of the School of Chemistry, University of Bristol.

The compounds $[Mo_2(\mu\text{-}C_8Me_8)(\eta\text{-}C_5H_5)_2]$, $[Mo_2(\mu\text{-}C_8Me_7CH_2D)(\eta\text{-}C_5H_5)_2]$, and $[Mo_2(\mu\text{-}C_8Me_7Et)(\eta\text{-}C_5H_5)_2]$,[6] $[Fe(\eta\text{-}C_5H_5)_2]$-

(15) Reuben, J.; Fiat, D. *J. Am. Chem. Soc.* **1969**, *91*, 1242.
(16) Diehl, P.; Leipert, T. *Helv. Chim. Acta* **1964**, *47*, 545.
(17) Johnson, A.; Everett, G. W., Jr. *J. Am. Chem. Soc.* **1970**, *92*, 6705.
(18) Horn, R. R.; Everett, G. W., Jr. *J. Am. Chem. Soc.* **1971**, *93*, 7173.
(19) Brown, N. C.; Carriedo, G. A.; Connelly, N. G.; Garcia Alonso, F. J.; Quarmby, I. C.; Rieger, A. L.; Rieger, P. H.; Riera, V.; Vivanco, M. *J. Chem. Soc., Dalton Trans.* **1994**, 3745.
(20) Smart, J. C.; Pinsky, B. L. *J. Am. Chem. Soc.* **1980**, *102*, 1009.

Table 4. Atomic Coordinates ($\times 10^4$) and Equivalent Isotropic Displacement Parameters ($Å^2 \times 10^3$) for $[Mo_2(\mu\text{-}C_8Me_8)(\eta\text{-}C_5H_5)_2][PF_6]$ ($1^+[PF_6]^-$)

	x	*y*	*z*	*U*(eq)
Mo(1)	3560(1)	2417(1)	5722(1)	22(1)
Mo(2)	4430(1)	2316(1)	6822(1)	22(1)
C(1)	3274(3)	1840(3)	6740(2)	28(1)
C(2)	3171(3)	1164(3)	6267(3)	29(1)
C(3)	3834(3)	995(3)	5837(2)	24(1)
C(4)	4653(3)	1051(3)	6170(2)	21(1)
C(5)	5157(3)	1670(3)	5906(2)	20(1)
C(6)	4830(3)	2211(3)	5338(2)	23(1)
C(7)	4756(3)	3106(3)	5470(2)	26(1)
C(8)	4481(3)	3321(3)	6126(2)	26(1)
C(1′)	2598(4)	2100(4)	7207(3)	51(2)
C(2′)	2408(3)	659(4)	6206(3)	44(1)
C(3′)	3774(3)	309(3)	5292(3)	34(1)
C(4′)	4916(3)	294(3)	6590(3)	34(1)
C(5′)	6052(3)	1689(3)	6022(3)	35(1)
C(6′)	5061(3)	1893(3)	4631(2)	35(1)
C(7)	4948(4)	3763(3)	4923(3)	46(2)
C(8′)	4361(4)	4248(3)	6322(3)	42(1)
C(17)	2557(6)	2124(5)	4918(5)	76(3)
C(18)	2213(4)	2443(5)	5455(5)	73(3)
C(19)	2442(4)	3259(4)	5574(4)	57(2)
C(20)	2968(4)	3497(4)	5088(4)	57(2)
C(21)	3073(5)	2756(8)	4638(3)	102(4)
C(22)	5056(6)	1800(5)	7825(3)	76(3)
C(23)	5527(4)	2477(6)	7589(4)	68(2)
C(24)	5067(4)	3206(4)	7621(3)	48(2)
C(25)	4325(4)	2995(4)	7874(3)	51(2)
C(26)	4309(5)	2110(5)	8004(3)	64(2)
P(1)	7074(1)	376(1)	1614(1)	47(1)
F(1)	7852(4)	807(7)	1394(4)	191(4)
F(2)	7403(6)	−529(5)	1592(5)	199(5)
F(3)	6290(4)	−30(6)	1836(5)	189(4)
F(4)	6890(5)	302(4)	847(3)	145(3)
F(5)	6702(6)	1248(4)	1576(4)	181(4)
F(6)	7298(8)	453(7)	2346(3)	258(7)

[a] *U*(eq) is defined as one-third of the trace of the orthogonalized $\mathbf{U}_{ij}$ tensor.

$[PF_6]$,[20] and 4-(triphenylmethyl)-1-(diphenylmethylidene)-2,5-cyclohexadiene (as a source of the radical $^{\bullet}CPh_3$)[21] were prepared by published methods.

$[Mo_2(\mu\text{-}C_8Me_8)(\eta\text{-}C_5H_5)_2][PF_6]$. To a stirred solution of $[Mo_2(\mu\text{-}C_8Me_8)(\eta\text{-}C_5H_5)_2]$ (0.20 g, 0.37 mmol) in CH_2Cl_2 (30 mL) was added a suspension of $[Fe(\eta\text{-}C_5H_5)_2][PF_6]$ (0.12 g, 0.36 mmol) in CH_2Cl_2 (10 mL). After 1 h the brown solution was evaporated to dryness and the residue was washed with hexane (50 mL). Slow diffusion of a layer of diethyl ether into a solution of the product in CH_2Cl_2 gave brown crystals, yield 0.21 g (85%). Anal. Calcd for $C_{26}H_{34}F_6Mo_2P$: C, 45.8; H, 4.9. Found: C, 45.6; H, 5.1.

The brown complexes $[Mo_2(\mu\text{-}C_8Me_7CH_2D)(\eta\text{-}C_5H_5)_2][PF_6]$ (Anal. Calcd for $C_{26}H_{33}DF_6Mo_2P$: C, 45.7; H, 5.0. Found: C, 45.6; H, 5.1) and $[Mo_2(\mu\text{-}C_8Me_7Et)(\eta\text{-}C_5H_5)_2][PF_6]$ (Anal. Calcd for $C_{27}H_{36}F_5Mo_2P$: C, 46.5; H, 5.2. Found: C, 46.1; H, 5.5) were prepared similarly, in 75 and 53% yield, respectively.

Reaction of $[Mo_2(\mu\text{-}C_8Me_8)(\eta\text{-}C_5H_5)_2][PF_6]$ with the Triphenylmethyl Radical. To a stirred solution of $[Mo_2(\mu\text{-}C_8Me_8)(\eta\text{-}C_5H_5)_2][PF_6]$ (20 mg, 29 μmol) in CH_2Cl_2 (10 mL) was added solid 4-(triphenylmethyl)-1-(diphenylmethylidene)-2,5-cyclohexadiene (as a source of the radical $^{\bullet}CPh_3$) (7 mg, 14 μmol). The brown solution became purple within 5 min but was stirred for a further 2 h and then evaporated to dryness. The residue was washed with *n*-hexane (50 mL) and then purified from CH_2Cl_2−diethyl ether to give $[Mo_2(\mu\text{-}C_8Me_7CH_2)(\eta\text{-}C_5H_5)_2][PF_6]$ as a purple solid, yield 18 mg (94%).

Reaction of $[Mo_2(\mu\text{-}C_8Me_8)(\eta\text{-}C_5H_5)_2][PF_6]$ with $[Fe(\eta\text{-}C_5H_5)_2][PF_6]$. To a stirred solution of $[Mo_2(\mu\text{-}C_8Me_8)(\eta\text{-}C_5H_5)_2][PF_6]$ (130 mg, 0.19 mmol) in CH_2Cl_2 (10 mL) was added $[Fe(\eta\text{-}C_5H_5)_2][PF_6]$ (70 mg, 0.21 mmol) in CH_2Cl_2 (10 mL). After 12 h the purple solution was evaporated to dryness and the residue was washed with *n*-hexane (50 cm^3). Purification from CH_2Cl_2−*n*-hexane gave $[Mo_2(\mu\text{-}C_8Me_7CH_2)(\eta\text{-}C_5H_5)_2][PF_6]$ as a purple solid, yield 108 mg (83%).

Crystal Structure Analysis of $1^+[PF_6]^-$. Crystal data for $[Mo_2(\mu\text{-}C_8Me_8)(\eta\text{-}C_5H_5)_2][PF_6]$ ($1^+[PF_6]^-$): $C_{26}H_{34}F_6Mo_2P$, M = 683.4, orthorhombic, space group *Pbca* (No. 61), a = 16.847(5) Å, b = 15.777(5) Å, c = 19.679(6) Å, V = 5231(3) $Å^3$, Z = 8, D_x = 1.74 g cm^{-3}, $\bar{\lambda}$ = 0.710 73 Å, μ = 1.08 mm^{-1}, $F(000)$ = 2744, T = 200 K. Diffraction measurements were made with a Siemens four-circle R3m/V diffractometer using graphite-monochromated Mo Kα X-radiation on a single crystal (approximate dimensions 0.23 × 0.50 × 0.45 mm) mounted in a thin-walled capillary under nitrogen. Cell dimensions were determined from the setting angle values of 28 centered reflections. A total of 5110 diffracted intensities (including checks) were measured in a unique octant of reciprocal space for $4.0 < 2\theta < 50.0°$ by Wyckoff ω scans. Three check reflections, remeasured after every 100 ordinary data, showed no decay and *ca*. 2% variation over the period of data collection. Of the noncheck intensity data collected, 4599 unique observations remained after averaging of duplicate and equivalent measurements and deletion of systematic absences; of these, 4595 with $I > -3\sigma(I)$ were retained for use in structure solution and refinement. An absorption correction was applied on the basis of 223 azimuthal scan data; maximum and minimum transmission coefficients were 0.835 and 0.575, respectively. Lorentz and polarization corrections were applied. The structure was solved by heavy atom (Patterson and difference Fourier) methods and refined by full-matrix least-squares against F^2. All non-hydrogen atoms were assigned anisotropic displacement parameters and refined without positional constraints. Hydrogen atoms were constrained to idealized geometries (C−H 0.96 Å) and assigned a fixed isotropic displacement parameter. An isotropic extinction correction was applied; parameter x refined to 0.0009(2), where $F_c = F_c^{uncorr}/(1 + 0.002xF_c^2/\sin 2\theta)^{1/4}$. Refinement of the 325 least-squares variables converged smoothly to residual indices $R1$ = 0.043 [for 3757 reflections with $I > 2\sigma(I)$], w$R2$ = 0.113, and S = 1.41 (for all 4595 data used in refinement).[22] Weights, w, were set equal to $[\sigma_c^2(F_o^2) + (gP)^2]^{-1}$, where $\sigma_c^2(F_o^2)$ = variance in F_o^2 due to counting statistics, $P = [\max(F_o^2,0) + 2F_c^2]/3$, and g = 0.05 were chosen to minimize the variation in S as a function of F_o. Final difference electron density maps showed no features outside the range +0.97 to −0.72 e $Å^{-3}$, the largest features being within 1 Å of the atoms of the anion. Table 4 reports the atomic positional parameters. Tables of atomic displacement parameters, hydrogen atom parameters, and bond distances and angles are given in the Supporting Information. All calculations were made with programs of the SHELXTL-PLUS package and SHELXL-93.[23] Complex neutral-atom scattering factors were taken from ref 24.

Acknowledgment. We thank the SERC for a Postdoctoral Research Associateship (to B.M.), Mr. M. Legge for help with EHMO calculations, and Dr. Martin Murray for help and advice with the NOE study.

Supporting Information Available: Tables of X-ray parameters, hydrogen positional and thermal parameters, anisotropic thermal parameters, and bond distances and angles (5 pages). Ordering information is given on any current masthead page.

OM950529I

(21) Volz, H.; Lotsch, W.; Schnell, H.-W. *Tetrahedron* **1970**, *26*, 5343.

(22) Residuals calculated as follows: w$R2 = [\sum w\Delta^2/\sum wF_o^4]^{0.5}$; $S = [\sum w\Delta^2/(NO - NV)]^{0.5}$; $R1 = \sum||F_o| - |F_c||/\sum|F_o|$; $\Delta = F_o^2 - F_c^2$; NO = number of observations; NV = number of variables.

(23) Sheldrick, G. M. SHELXTL-PLUS, Rev. 4.2, Göttingen, FRG, 1990. SHELXL93: Sheldrick, G. M. *J. Appl. Crystallogr.* **1995**, in preparation.

(24) *International Tables for Crystallography*; Kluwer: Dordrecht, The Netherlands, 1992; Vol. C.